Supporting Information

Self-protected CeO_2-SnO_2@SO_4^{2-}/TiO_2 Catalysts with Extraordinary Resistance to Alkali and Heavy Metals for NO_x Reduction

Sixiang Cai,[†, ‡, §] Tuoyu Xu,[†, ‡, §] Penglu Wang,[†, §] Lupeng Han,[†] Sarawoot Impeng[Ψ], Yue Li,[‡] Tingting Yan,[†] Guorong Chen,[†] Liyi Shi[†] and Dengsong Zhang*[,†]

[†]International Joint Laboratory of Catalytic Chemistry, Department of Chemistry, Research Center of Nano Science and Technology, College of Sciences, Shanghai University, Shanghai 200444, China.

[‡]State Key Laboratory of Marine Resource Utilization in South China Sea, School of Materials Science and Engineering, Hainan University, Haikou 570228, Hainan, China.

[Ψ]National Nanotechnology Center, National Science and Technology Development Agency, Pathum Thani 12120, Thailand.

[§]These authors contributed equally to this work.

*Corresponding Author. E-mail: dszhang@shu.edu.cn; Tel: +86-21-66137152.

The Supporting Information includes 29 pages, 16 figures, and 4 tables.

Table of Contents

Catalytic Performance

SCR activity tests were performed on a multi-function catalyst characterization system (VDRT-200SMT). The powders of catalysts were pressed, crushed and sieved to 20-40 mesh, then the processed samples were put into a quartz tube with 8 mm inside diameter. The reactant gases were as follow: 500 ppm NO, 500 ppm NH_3, 5% O_2, 8 vol% H_2O (when used), 100 ppm SO_2 (when used) and N_2 (be used as carrier gas). The concentrations of outlet gas (NO, NO_2, N_2O, NH_3) were recorded by an FTIR spectrometer (Thermo Fisher). The NO conversion, N_2 selectivity and specific reaction rate were calculated by the following equations[1]:

$$NO_x\ conversion(\%)=\frac{[NO_x]_{in}-[NO_x]_{out}}{[NO_x]_{in}}\times 100\% \quad (1)$$

$$N_2\ selectivity(\%)=\left(1-\frac{2[N_2O]}{[NH_3]_{in}+[NO_x]_{in}-[NH_3]_{out}-[NO_x]_{out}}\right)\times 100\% \quad (2)$$

Where $[NO_x]_{in}$ (ppm) and $[NO_x]_{out}$ (ppm) are the inlet and outlet gas NO_x concentration, $[NH_3]_{in}$ (ppm) and $[NH_3]_{out}$ (ppm) are the inlet and outlet gas NH_3 concentration and $[N_2O]$ (ppm) is the outlet gas N_2O concentration, respectively.

$$Specific\ reaction\ rate=\frac{\frac{PV}{RT}\cdot Q\cdot X_{NO_x}}{w\cdot S_{BET}} \quad (3)$$

Where P=1.01 MPa, V=22.4 L/mol, R=8.314 J/mol^{-1}·K^{-1} , T refers to the test temperature (K), Q is volume velocity (ml/min), X_{NOx} is NO_x conversion, w is the mass of the catalyst and S_{BET} is the specific surface area of the catalyst, respectively.

Bond Force Constant

The Ti-O bond force constant is obtained by the follow Formula:[2]

$$\omega=\frac{1}{2\pi c}\sqrt{\frac{k}{\mu}}$$

where ω is the Raman shift (cm^{-1}), c is light velocity, and μ is effective mass.

Catalytic Characterization

Morphology. Scanning electron microscope (SEM) images were photoed by a field-emission scanning electron microscopy (FE-SEM, SIGMA-300). EDS (Energy Dispersive Spectroscopy) mapping of catalysts were completed on Oxford Instruments EDS.

Textural and Structural Properties. X-ray diffraction (XRD) was performed on an X-ray diffractometer (3KW D/MAX2200V PC, Japan) with a scan speed of 8 $^{o}\cdot min^{-1}$.[3] The Raman (LabRAM HR Evolution, Horiba, France) test was obtained by using Raman spectrometer with the laser at 532 nm as the excitation source.[4] X-ray photoelectron spectrometry (XPS) was carried out on an X-ray photoelectron spectrometer (Thermo Scientific, ESCALAB250Xi), all binding energies were corrected by the containment carbon peak (C 1s = 284.6 eV).[5] Nitrogen adsorption-desorption isotherms were recorded by a specific surface area and porosity analyzer (micromeritics, ASAP 2460). The catalysts were put into Dewar flask to de-gas by a micromeritics sample degas system (VacPrep 061) for 12h at 300 ^{o}C. The mesopore sizes were calculated by Barrett-Joyner-Halenda (BJH) method.[6] The XPS sputtering experiment was tested by a X-ray photoelectron spectroscopy (ThermoFischer, ESCALAB 250Xi). Among them, the vacuum of the analysis chamber is 8×10^{-10} pa, the excitation source is Al ka ray (hv=1486.8 eV), the operating voltage is 12.5 kV, the filament current is 16 mA, and the signals are accumulated for 5 cycles. Argon ion gun is used to clean the surface, the spot size is a circle with diameter 2 mm, ion energy is 3000 eV, etching time is 1 min, Passing-Energy is 40 eV, step length is 0.1 eV, charge correction is carried out with C1s=284.60 eV binding energy as energy standard.

Chemisorption Properties. The Ammonia temperature-programmed desorption (NH_3-TPD) tests were performed on a Micromeritics AutoChem 2920 II instrument with thermal conductivity

detector (TCD).[7] First, catalyst powder (80 mg) were put into a U-shaped quartz tube and pretreated in the He gas flow of 30 ml·min^{-1} for 30 minutes at 100 ^{o}C. After cooling to 100 ^{o}C, the samples was exposed to NH_3/He atmosphere for 1 hour. Then the catalyst was purged by He for 1 h at this temperature to remove the physically adsorbed NH_3 on the surface of samples. Finally, the temperature was raised to 850 ^{o}C by a heating rate of 10 ^{o}C·min^{-1}, meanwhile, the desorption curve of NH_3 was recorded. The hydrogen temperature-programmed reduction (H_2-TPR) tests were performed on the Micromeritics AutoChem 2920 II instrument as well. First, catalyst powder (80 mg) was put into a U-shaped quartz tube and pretreated in the He gas flow of 30 ml·min^{-1} for 30 minutes at 100 ^{o}C. After cooling to room temperature, the samples were exposed to H_2/Ar atmosphere, then the temperature was raised to 750 ^{o}C by a rate of 10 ^{o}C·min^{-1} and the reduction curve was recorded.

Infrared Spectroscopy. Both of pyridine-infrared spectroscopy (IR) and in situ diffuse reflectance infrared Fourier transform spectroscopy (in situ DRIFTs) experiments were performed on a Nicolet 6700 spectrometer with a liquid nitrogen cooled mercury cadmium telluride (MCT) detector.[8] The DRIFTs spectra were collected in the range of 1000-1800 cm^{-1} in Kubelka-Munk format, accumulating 64 scans at 4 cm^{-1} resolution. First, each catalysts were pretreated at 300 °C for 30 min under a 30 ml·min^{-1} N_2 flow. After cooling to 100 ^{o}C, record this spectra as background. The catalysts were exposed to 500ppm NH_3 (NO + O_2) for 1h, deducted the background and recorded the spectra. Then the ingas was switched to N_2 to remove the physically adsorbed NH_3 (nitrate) species. Finally, N_2 was turned off and 500ppm NO + O_2 (NH_3) was introduced, meanwhile the spectrum were recorded by a frequency of once a minute until 20 min.

Computational method and model for DFT calculations

Spin-polarized DFT calculations were carried out using the Vienna *Ab initio* Simulation Package

(VASP).[9] The Perdew-Burke-Ernzerhof (PBE) functional and the projector augmented wave (PAW) method were used. [10, 11] To account for van der Waals (vdW) interaction, the DFT-D3 method of Grimme was utilized.[12] For geometry optimizations, the force and energy convergences were 0.02 eV/Å and 10^{-5} eV, respectively. A plane wave energy cutoff was opted at 400 eV. Brillouin zone sampling was performed using a 3 × 3 × 1 Monkhorst-Pack grid.[13] The DFT + U was applied to address the on-site Coulomb interaction with the U-J parameters of 3.5 eV for Ti 3d.[14]

The TiO_2 (101) and $Ti(SO_4)_2$ $(21\bar{3})$ surfaces were modeled using periodic slabs of (1 × 3) and (1 × 1), respectively. A vacuum space of 18 Å was added in the direction perpendicular to the surface to prevent interactions between periodic images.

The combination energy of each chemical species on catalyst surfaces is defined as:

$$E_{com} = E_{species/surface} - (E_{species} + E_{surface})$$

where $E_{species/surface}$ is the total energy of species/surface complex, and $E_{species}$ and $E_{surface}$ are the total energies of corresponding species and surface, respectively. Accordingly, the more negative value indicates the stronger combination.

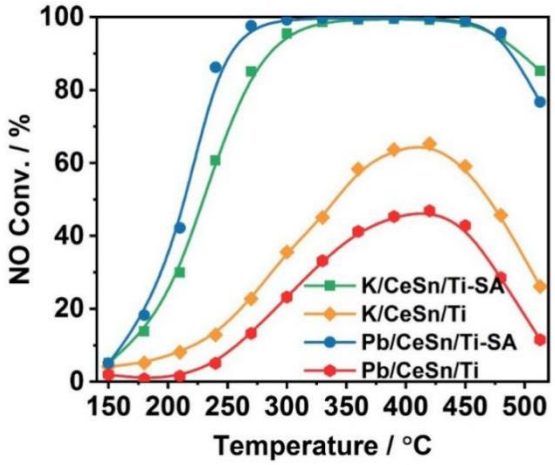

Figure S1. Plots of NO_x conversion *versus* temperature for K/CeSn/Ti-SA, K/CeSn/Ti, Pb/CeSn/Ti-SA and Pb/CeSn/Ti. Reaction conditions: 500 ppm NO, 500 ppm NH_3, 5 vol % O_2, N_2 as the balance gas, and GHSV of 50,000 h^{-1}.

For CeSn/Ti-SA catalysts, only a slight decrease of the NH_3-SCR activity can be observed at low temperature range after the loading of K or Pb. On the contrary, the maximum de-NO_x performance of CeSn/Ti catalysts only preserved about 60% and 43% after K and Pb poisoning, respectively.

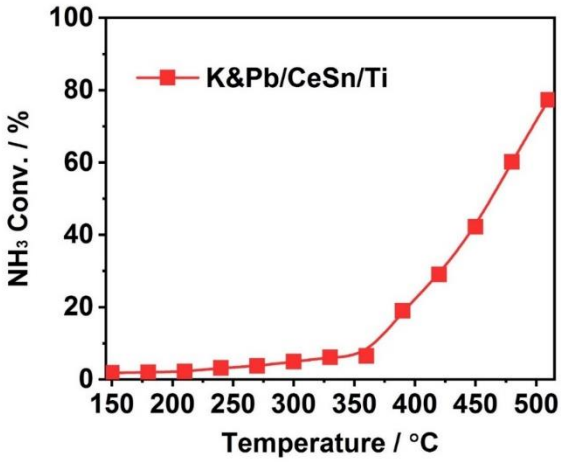

Figure S2. Plots of NH_3 conversion *versus* temperature for K&Pb/CeSn/Ti-SA catalysts. Reaction conditions: 500 ppm NH_3, 5 vol % O_2, N_2 as the balance gas, and GHSV of 50,000 h^{-1}.

Since the acid sites on the surface of CeSn/Ti were consumed after K&Pb co-poisoning, the adsorbption of NO become easier than NH_3, leading to the reaction of NH_3 oxidation at higher temperatures and the decrease of N_2 selectivity.[15]

NH_3 conversion was calculated by the following equality:[16]

$$NH_3\ conversion(\%)=\frac{[NH_3]_{in}-[NH_3]_{out}}{[NH_3]_{in}}\times 100\%$$

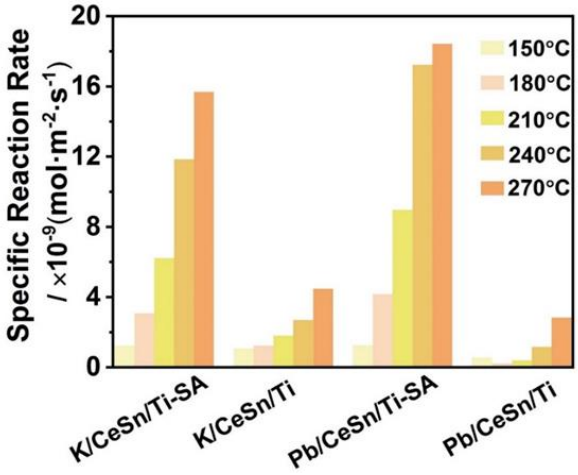

Figure S3. Plots of specific reaction rates over different temperature for K/CeSn/Ti-SA, K/CeSn/Ti, Pb/CeSn/Ti-SA and Pb/CeSn/Ti.

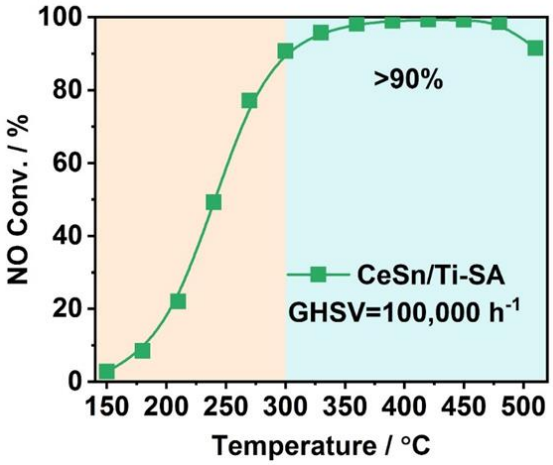

Figure S4. Plots of NO conversion as a function of reaction temperature for the catalysts of CeSn/Ti-SA. Reaction conditions: 500 ppm NO, 500 ppm NH_3, 5 vol % O_2, N_2 as the balance gas, and GHSV of 100,000 h^{-1}.

CeSn/Ti-SA catalysts hold an activity above 90% within the range of 300~510°C under high GHSV of 100,000 h^{-1}.

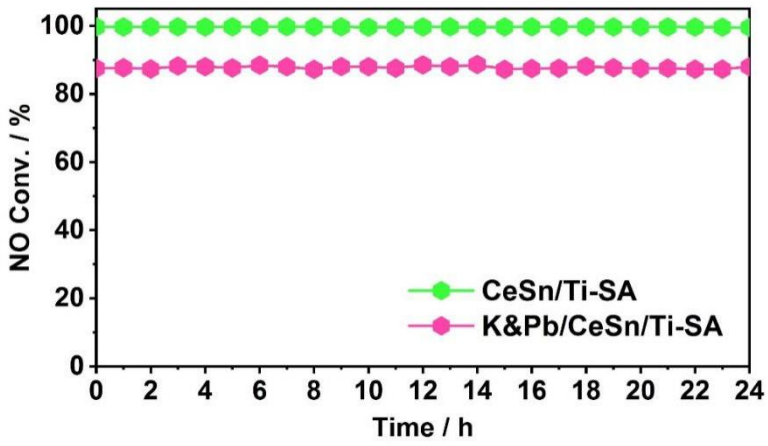

Figure S5. Plots of stability test for CeSn/Ti-SA and K&Pb/ CeSn/Ti-SA at 300°C for 24 h. Reaction conditions: 500 ppm NO, 500 ppm NH_3, 5 vol % O_2, N_2 as the balance gas, and GHSV of 50,000 h^{-1}.

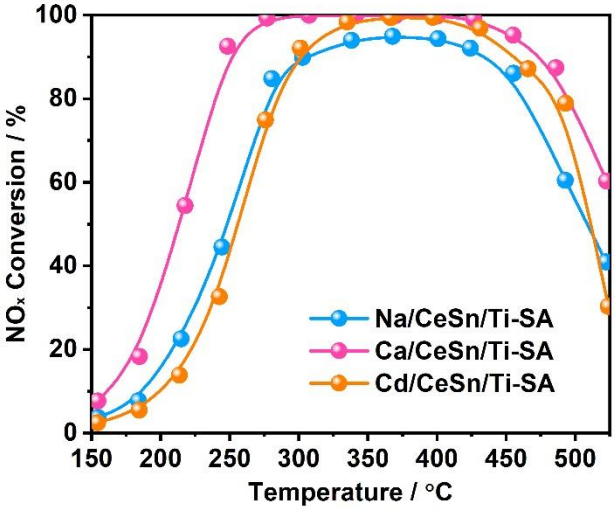

Figure S6. Plots of NO_x conversion *versus* temperature for Na/CeSn/Ti-SA, Ca/CeSn/Ti and Cd/CeSn/Ti-SA. Reaction conditions: 500 ppm NO, 500 ppm NH_3, 5 vol % O_2, N_2 as the balance gas, and GHSV of 50,000 h^{-1}.

Since Na is one of the main components of alkali metals in fly ash, Ca is the main component of alkaline earth metals in fly ash, and Cd is the heavy metal in municipal solid waste incinerator second only to Pb. It is of great significance to investigate the resistance of catalysts to these poisons.[17] The results in Figure S6 shown that the CeSn/Ti-SA catalysts had good resistance to Na, Ca and Cd. Among these three poisons, CaO had the least effect on the activity of the catalyst, followed by CdO and Na_2O. The effect of CaO on the activity of the catalyst was mainly concentrated in the high temperature section, especially the activity decreased obviously above 450°C. While the effects of CdO and Na_2O on the catalysts were not only at high temperature but also at low temperature.

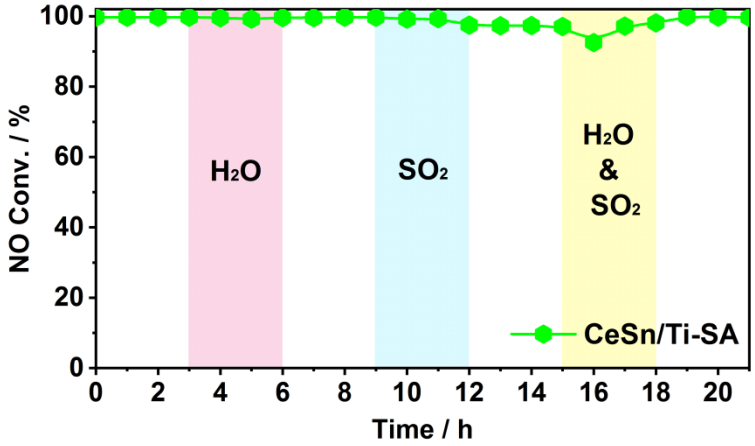

Figure S7. Plots of H_2O, SO_2 and H_2O&SO_2 durability test for the CeSn/Ti-SA catalyst at 300 °C. Reaction conditions: 500 ppm NO, 500 ppm NH_3, 5 vol % O_2, 8 vol % H_2O (when used), 100 ppm SO_2 (when used), N_2 as the balance gas, and GHSV of 50,000 h^{-1}.

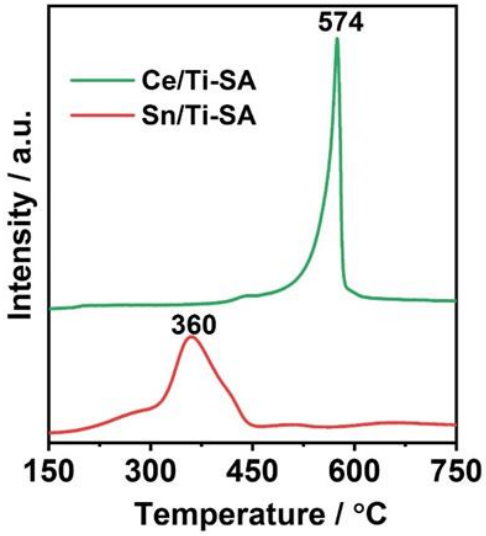

Figure S8. H_2-TPR curves of Ce/Ti-SA and Sn/Ti-SA.

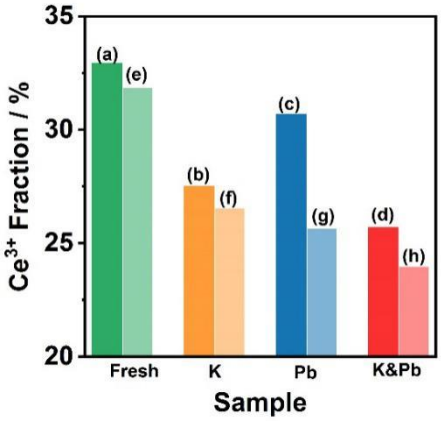

182

183 **Figure S9.** Ce^{3+} fraction obtained by the XPS spectra of Ce 3d for (a) CeSn/Ti-SA, (b) K/CeSn/Ti-SA,

184 (c) Pb/CeSn/Ti-SA, (d) K&Pb/CeSn/Ti-SA, (e) CeSn/Ti, (f) K/CeSn/Ti, (g) Pb/CeSn/Ti and (h)

185 K&Pb/CeSn/Ti.

186

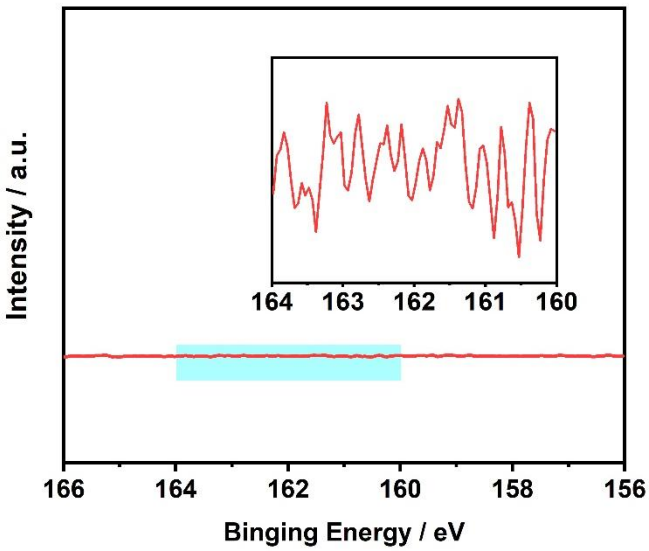

Figure S10. XPS spectra of S 2p for CeSn/Ti-SA at ~162 eV. The inset is the magnified one of the blue zone.

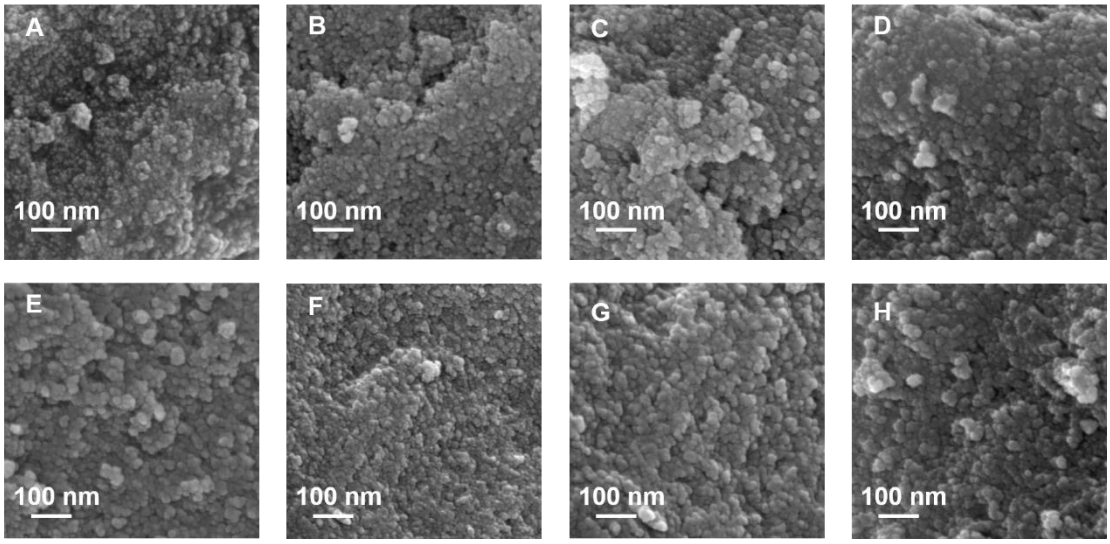

Figure S11. SEM images of (A) CeSn/Ti-SA, (B) K/CeSn/Ti-SA, (C) Pb/CeSn/Ti-SA, (D) K&Pb/CeSn/Ti-SA, (E) CeSn/Ti, (F) K/CeSn/Ti, (G) Pb/CeSn/Ti and (H) K&Pb/CeSn/Ti.

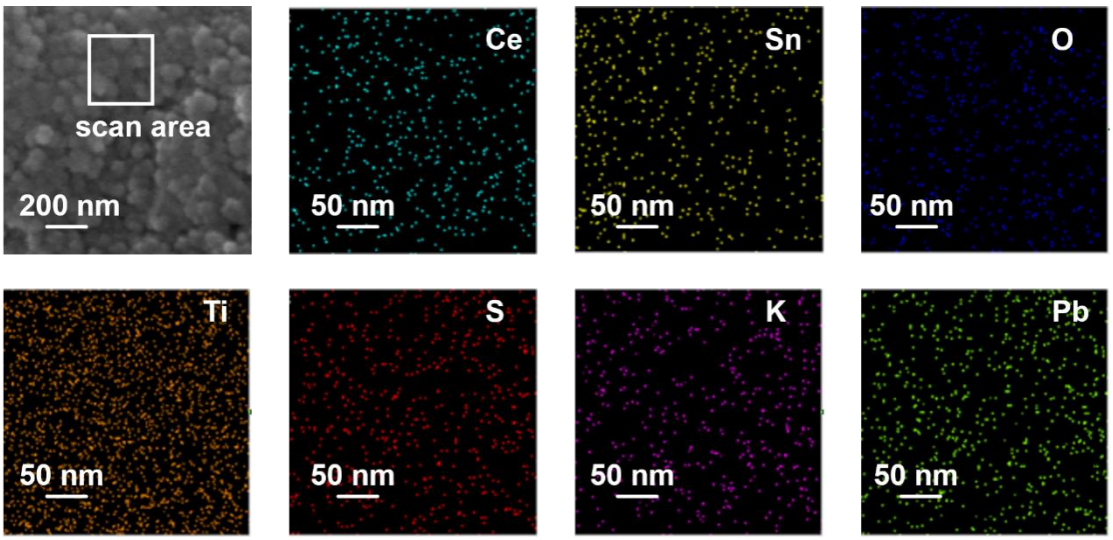

Figure S12. EDS mapping of the K&Pb/CeSn/Ti-SA.

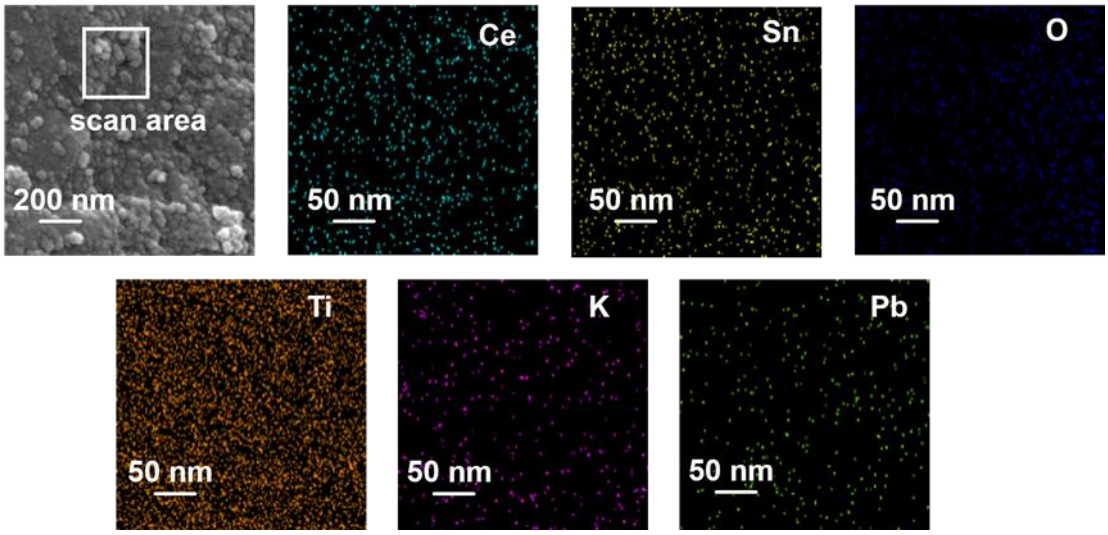

Figure S13. EDS mapping of the K&Pb/CeSn/Ti.

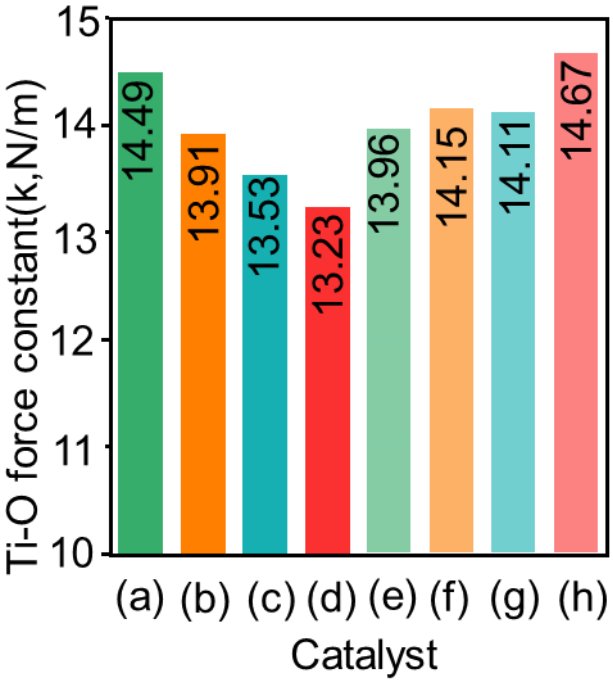

Figure S14. The Ti-O bond force constant in Eg (v6) mode of anatase phase TiO_2 for (a) CeSn/Ti-SA, (b) K/CeSn/Ti-SA, (c) Pb/CeSn/Ti-SA (d) K&Pb/CeSn/Ti-SA, (e) CeSn/Ti, (f) K/CeSn/Ti, (g) Pb/CeSn/Ti and (h) K&Pb/CeSn/Ti,

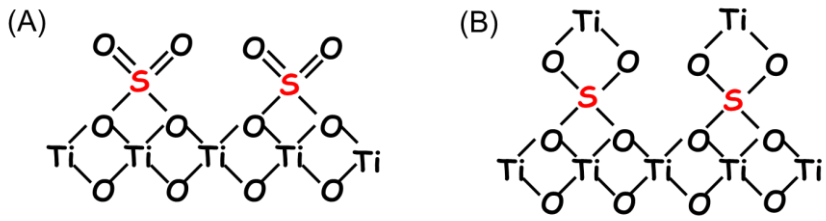

Figure S15. The bonding state of (A) sulfates on the surface of titanium dioxide and (B) sulfates in the bulk phase of titanium dioxide.

Referring to the bonding mode of sulfate on the surface of zirconium dioxide in the literatures of *J. Colloid Interface Sci.* **2013***, 394,* 515-521 and *J. Phys. Chem. C* **2015**, 119, 15077-15084, similarly, we establish the DFT model of sulfate bonding on the surface of titanium dioxide by placing sulfate groups on the surface of titanium dioxide (Figure S15A), in which only one kind of bonding state of S-O-Ti bonds existed.[17,18] However, there are other possibilities for the bonding state between sulfate and titanium dioxide, especially in the bulk phase, as the bonding mode shown in Figure S15B, which was very close to the bonding state in titanium sulfate. Therefore, the model of $Ti(SO_4)_2$ was selected as the ideal cases of sulfates present more in the bulk phase of TiO_2.

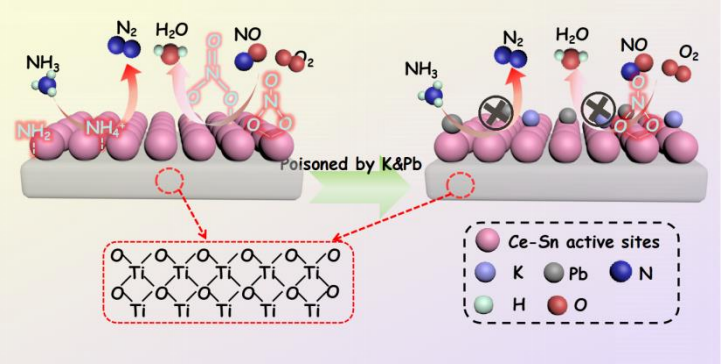

Figure S16. The deactivation mechanism of K&Pb/CeSn/Ti.

223 **Table S1.** Specific surface areas (S_{BET}: m^2/g) of fresh and poisoned catalysts.

Catalyst	Fresh	Pb-poisoned	K-poisoned	K&Pb co-poisoned
CeSn/Ti-SA	102	86	84	79
CeSn/Ti	101	81	75	66

224

225 **Table S2.** The amount of NH_3 desorption (mmol/g) of fresh and poisoned catalysts.

Sample	Weak acid	Middle acid	Strong acid	Super acid
CeSn/Ti-SA	0.46571	0.12059	/	1.119
K/CeSn/Ti-SA	0.44076	0.10795	/	0.63698
Pb/CeSn/Ti-SA	0.4497	0.10031	/	0.62323
K&Pb/CeSn/Ti-SA	0.3062	0.00723	/	0.32073
CeSn/Ti	0.45294	0.12058	0.04328	/
K/CeSn/Ti	0.11923	0.00285	/	/
Pb/CeSn/Ti	0.26007	0.02748	0.00722	/
K&Pb/CeSn/Ti	0.09771	0.00211	/	/

226 These data was obtained from NH_3-TPD results.

227

Table S3. Normalized Brønsted acid and Lewis acid (μmol/g) of fresh and poisoned catalysts.

Sample	Lewis acid			Brønsted acid	
	1444 cm^{-1}	1575 cm^{-1}	1602 cm^{-1}	1540 cm^{-1}	1640 cm^{-1}
CeSn/Ti-SA	204	60	226	134	187
K/CeSn/Ti-SA	187	55	154	110	172
Pb/CeSn/Ti-SA	105	48	102	74	126
K&Pb/CeSn/Ti-SA	91	26	86	40	68
CeSn/Ti	161	58	124	/	137
K/CeSn/Ti	71	32	62	/	27
Pb/CeSn/Ti	103	60	100	/	23
K&Pb/CeSn/Ti	58	19	56	/	14

These data was obtained from Py-IR results.

The Normalized Lewis acid and Brønsted acid were calculated by the following equations:[20]

$C(\text{pyridine on B sites}) = 1.88IA(B)R^2/W$

$C(\text{pyridine on L sites}) = 1.42IA(L)R^2/W$

IA(B.L) = integrated absorbance of B or L band (cm^{-1})

R = radius of catalyst disk (cm^{-1})

W = weight of sample (mg)

Table S4. Atomic ratio of each element divided by titanium atom.

Sample	Ce/Ti	Sn/Ti	O/Ti	S/Ti	Pb/Ti	K/Ti
CeSn/Ti-SA	0.0950	0.0971	2.3638	/	/	/
K/CeSn/Ti-SA	0.1338	0.0916	2.5123	0.0859	/	0.0104
Pb/CeSn/Ti-SA	0.1109	0.0616	2.4425	0.0993	0.0198	/
K&Pb/CeSn/Ti-SA	0.1416	0.0827	2.6579	0.1309	0.0278	0.0507

These data was obtained from XPS results.

References

(1) Huang, L.; Zha, K.; Namuangruk, S.; Junkaew, A.; Zhao, X.; Li, H.; Shi, L.; Zhang, D., Promotional effect of the TiO_2 (001) facet in the selective catalytic reduction of NO with NH_3: in situ DRIFTS and DFT studies. *Catal. Sci. Technol.* **2016**, *6*, (24), 8516-8524.

(2) Rong, S.; Zhang, P.; Liu, F.; Yang, Y., Engineering crystal facet of α-MnO_2 nanowire for highly efficient catalytic oxidation of carcinogenic airborne formaldehyde. *ACS Catal.* **2018**, *8*, (4), 3435-3446.

(3) Yoo, J. S.; Bhattacharyya, A. A.; Radlowski, C. A., De-SO_x catalyst: an XRD study of magnesium aluminate spinel and its solid solutions. *Ind. Eng. Chem. Res.* **1991**, *30*, (7), 1444-1448.

(4) Akins, D. L.; Macklin, J. W.; Zhu, H. R., ChemInform abstract: visible Raman and near-infrared fourier transform raman characterization of adsorbed 4,4′-cyanine. *J. Phys. Chem. C* **1992**, *96*, (11): 4515-4521.

(5) Gardner, T. H.; Spivey, J. J.; Kugler, E. L.; Campos, A.; Hissam, J. C.; Roy, A. D., Structural characterization of ni-substituted hexaaluminate catalysts using E EXAFS, XANES, XPS, XRD, and TPR. *J. Phys. Chem. C* **2010**, *114*, (17), 7888-7894.

(6) Strømme, M.; Mihranyan, A.; Ek, R.; Niklasson, G. A., Fractal dimension of cellulose powders analyzed by multilayer BET adsorption of water and nitrogen. The *J. Phys. Chem. B* **2003**, *107*, (51), 14378-14382.

(7) Watanabe, S.; Ma, X.; Song, C., Characterization of structural and surface properties of nanocrystalline TiO_2− CeO_2 mixed oxides by XRD, XPS, TPR, and TPD. *J. Phys. Chem. C* **2009**, *113,* (32): 14249-14257.

(8) Wang, X.; Liu, Y.; Zhang, T.; Luo, Y.; Lan, Z.; Zhang, K.; Zuo, J.; Jiang, L.; Wang, R., Geometrical-site-dependent catalytic activity of ordered mesoporous Co-based spinel for benzene oxidation: in situ DRIFTS study coupled with Raman and XAFS spectroscopy. *ACS Catal.* **2017**, *7*, (3), 1626-1636.

(9) Kresse, G.; Furthmüller, J., Efficient iterative schemes for ab initio total-energy calculations using a plane-wave basis set. *Phys. Rev. B* **1996,** *54*, (16), 11169-11186.

(10) Perdew, J. P.; Burke, K.; Ernzerhof, M., Generalized Gradient Approximation Made Simple. *Phys. Rev. Lett.* **1996,** *77*, (18), 3865-3868.

(11) Kresse, G.; Joubert, D., From ultrasoft pseudopotentials to the projector augmented-wave method. *Phys. Rev. B* **1999,** *59*, (3), 1758-1775.

(12) Grimme, S.; Antony, J.; Ehrlich, S.; Krieg, H., A consistent and accurate ab initio parametrization of density functional dispersion correction (DFT-D) for the 94 elements H-Pu. *J. Chem. Phys* **2010**, *132*, (15), 154104.

(13) Monkhorst, H. J.; Pack, J. D., Special points for Brillouin-zone integrations. *Phys. Rev. B* **1976,** *13*, (12), 5188-5192.

(14) Dudarev, S. L.; Botton, G. A.; Savrasov, S. Y.; Humphreys, C. J.; Sutton, A. P., Electron-energy-loss spectra and the structural stability of nickel oxide: An LSDA+U study. *Phys. Rev. B* **1998,** *57*, (3), 1505-1509.

(15) Han, L.; Gao, M.; Hasegawa, J. Y.; Li, S.; Shen, Y.; Li, H.; Shi, L.; Zhang, D., SO_2-Tolerant selective catalytic reduction of NO_x over meso-TiO_2@Fe_2O_3@Al_2O_3 metal-based monolith catalysts. *Environ. Sci. Technol.* **2019**, *53*, (11), 6462-6473.

(16) Wang, P.; Chen, S.; Gao, S.; Zhang, J.; Wang, H.; Wu, Z., Niobium oxide confined by ceria nanotubes as a novel SCR catalyst with excellent resistance to potassium, phosphorus, and lead. *Appl. Catal., B: Environ.* **2018,** *231*, 299-309.

(17) Lin, M.; An, B.; Niimi, N.; Jikihara, Y.; Nakayama, T.; Honma, T.; Takei, T.; Shishido, T.; Ishida, T.; Haruta, M.; Murayama, T., Role of the acid site for selective catalytic oxidation of NH_3 over Au/Nb_2O_5. *ACS Catal.* **2019**, *9*, (3), 1753-1756.

(18) Gao, S.; Chen, X.; Wang, H.; Mo, J.; Wu, Z.; Liu, Y.; Weng, X., Ceria supported on sulfated zirconia as a superacid catalyst for selective catalytic reduction of NO with NH_3. *J. Colloid Interface Sci*. **2013**, *394*, 515-521.

(19) Wang, H.; Gao, S.; Yu, F.; Liu, Y.; Weng, X.; Wu, Z. Effective way to control the performance of a ceria-based deNO_x catalyst with improved alkali resistance: acid–base adjusting. *J. Phys. Chem. C* **2015**, *119*, (27), 15077-15084.

(20) Zhifei Hao, Z. S., Yi Li, Haitao Wang, Lirong Zheng, Ruihua Wang, Guoquan Liu, and; Zhan, S., The role of alkali metal in α-MnO_2 catalyzed ammonia‐selective catalysis. *Angew. Chem. Int. Ed.* **2019**, *58*, 6351 -6356.